

UxNB-Enabled Cell-Free Massive MIMO with HAPS-Assisted Sub-THz Backhauling

Omid Abbasi, *Graduate Student Member, IEEE*, Halim Yanikomeroglu,
Fellow, IEEE

Abstract

In this paper, we propose a cell-free scheme for unmanned aerial vehicle (UAV) base stations (BSs) to manage the severe intercell interference between terrestrial users and UAV-BSs of neighboring cells. Since the cell-free scheme requires enormous bandwidth for backhauling, we propose to use the sub-terahertz (sub-THz) band for the backhaul links between UAV-BSs and central processing unit (CPU). Also, because the sub-THz band requires a reliable line-of-sight link, we propose to use a high altitude platform station (HAPS) as a CPU. At the first time-slot of the proposed scheme, users send their messages to UAVs at the sub-6 GHz band. The UAVs then apply match-filtering and power allocation. At the second time-slot, at each UAV, orthogonal resource blocks are allocated for each user at the sub-THz band, and the signals are sent to the HAPS after analog beamforming. In the HAPS receiver, after analog beamforming, the message of each user is decoded. We formulate an optimization problem that maximizes the minimum signal-to-interference-plus-noise ratio of users by finding the optimum allocated power as well as the optimum locations of UAVs. Simulation results demonstrate the superiority of the proposed scheme compared with aerial cellular and terrestrial cell-free baseline schemes.

Index Terms

UxNB, cell-free, HAPS, THz, backhaul.

I. INTRODUCTION

The application of unmanned aerial vehicles (UAVs) as base stations (BSs), which are called UxNBs by the third generation partnership project (3GPP) [1], has attracted substantial attention

This work was supported by Huawei Canada Co., Ltd.

O. Abbasi and H. Yanikomeroglu are with the Department of Systems and Computer Engineering, Carleton University, Ottawa, ON K1S5B6, Canada. e-mail: omidabbasi@sce.carleton.ca; halim@sce.carleton.ca (*Corresponding author: Omid Abbasi*)

for 5G and beyond-5G due to their many advantages, such as high mobility, on-demand deployment, and a high probability of establishing a line-of-sight (LoS) link with users. UxNBs can provide connectivity for users at special events, such as those held in stadiums or theatres, or in areas impacted by natural disasters like floods or earthquakes. These scenarios can be in served, under-served or un-served areas. Deploying UxNBs can also be very useful in cases where terrestrial infrastructure may be unable to serve all users due to a temporary spike in demand. At such cases, some users can be offloaded to the aerial infrastructure. While LoS connectivity between each UxNB and users can provide very high data rates for the users within cell, severe intercell interference in aerial cellular networks [2], which is caused by UxNBs of neighboring cells, is a big problem. Another challenge of utilizing UxNBs is their backhauling, and since this can not be performed through the fiber link; it must be wireless [3]. Backhauling challenge of UxNBs is even greater in remote areas, where terrestrial infrastructure or fiber links may be lacking. In this paper, we solve these two challenges of UxNBs, i.e., intercell interference and backhauling, with the aid of the cell-free [4] scheme and a High altitude platform station (HAPS) [5], respectively.

Cell-free massive multiple input multiple output (MIMO) is a technology that has been proposed for beyond 5G [4]. In this technology, each user is served by a massive number of access points (APs), and all of these APs are connected to a central processing unit (CPU) [6]. In this method, the interference from other cells is utilized as the desired signal, and all of these received signals of APs are combined at the CPU. In our work, we propose to apply this cell-free scheme for a set of aerial APs (UxNBs) to manage the severe intercell interference in aerial cellular networks between UxNBs of neighboring cells and terrestrial users. There are many works in the literature that investigate cell-free scheme for terrestrial networks [4], [6]–[8]. However, to the best of our knowledge, our work is the first to consider the cell-free scheme for the UAV-BSSs.

In the cell-free scheme, enormous bandwidth is required for the backhaul links between APs and CPU. For terrestrial cell-free APs, this huge bandwidth for backhauling can be provided by fiber links [6], [7]. However, for our proposed aerial cell-free APs, this backhauling must be wireless. In order to satisfy the enormous bandwidth requirements of backhauling for UxNBs, we need to utilize the upper frequency bands for these wireless links [3]. In [9], in order to address the limited wireless backhaul capacity of UxNBs and consequently, decrease the latency, content caching is proposed to alleviate the backhaul congestion. The authors in [10] provided analytical

expressions for the probability of successfully establishing a backhaul link in the millimeter-wave band between UAV-BSs and ground stations, and they showed that increasing the density of the ground station network improved the performance of the backhauling. In [2], the authors proposed utilizing the coordinate multipoint scheme for UAV-BSs in uplink communications. They assumed that the backhaul links between all UAVs and the CPU were perfect so that the signal distortion induced by the backhaul transmission was ignored. The problem of wireless backhauling of UxNBs is largely due to the dynamic blockages and shadowing between UxNBs and a terrestrial CPU, which makes it difficult to utilize the upper frequency bands (such as, the terahertz (THz) band) for these links [11]. Higher frequency bands require a reliable LoS link, and probabilistic LoS links between UAVs and a terrestrial CPU is not suitable for these bands. We propose to utilize a HAPS in the stratosphere to solve this problem.

The application of HAPSs in wireless networks has attracted a lot of attention recently [5], [12], [13]. HAPSs are typically deployed in the stratosphere at an altitude of around 20 km with a quasi-stationary position relative to the earth [14]. A HAPS can provide LoS communication and a wide coverage radius of 50 – 500 km, and it can be equipped with powerful computing resources and batteries [5]. In [15], the authors envisioned a HAPS as a super macro base station to provide connectivity in a plethora of applications. Unlike a conventional HAPS, which targets broad coverage for remote areas or disaster recovery, they envisioned HAPS for highly populated metropolitan areas. In [16], HAPS computing was considered as a promising extension of the edge computing. The authors in [17] envisioned a HAPS as an enabling technology for communication, computing, caching, and sensing in the next-generation aerial delivery networks. In [18], the authors analyzed the link budget of the aerial platforms equipped with reconfigurable smart surfaces, and compared their communication performance with that of the terrestrial networks. In our scheme, instead of a terrestrial CPU, we propose to utilize a HAPS as an aerial CPU to process all the received signals from all UxNBs. HAPS is an ideal choice to work as a CPU for our proposed cell-free scheme since there is negligible blockage and shadowing for backhaul links between a HAPS and UxNBs, which means the LoS links will be reliable. Hence, we can easily use the upper frequency bands for these links to support the enormous bandwidth requirement for backhauling of the proposed cell-free scheme. In addition to backhauling of the UxNBs in the urban and dense urban environments, another important scenario for using a HAPS as a CPU for backhauling of the aerial APs is for the cases where these APs are deployed to serve users in remote areas or where terrestrial infrastructure and fiber links may be lacking

or damaged.

In this paper, we propose to use the sub-THz frequency band for the backhaul links between UxNBs and HAPS. The THz band is generally defined as the region of the electromagnetic spectrum in the range of 100 GHz to 10 THz, and sub-THz band is defined as the frequencies in the range of 100 GHz to 300 GHz [19], [20]. The D band (110 – 170 GHz) is among the next interesting range of frequencies for beyond-5G systems [21], [22], and hence we consider this band as the carrier frequency in our paper. The authors in [23] developed an analytical model for interference and signal-to-interference-plus-noise ratio (SINR) assessment in dense THz networks obtaining the first two moments and density functions for both metrics. In [24], the authors investigated a THz Ultra-Massive-MIMO-based aeronautical communication scheme for the space-air-ground integrated network. In [25], the problem of UAV deployment, power allocation, and bandwidth allocation was investigated for a UAV-assisted wireless system operating at THz frequencies.

The main contributions of this paper are summarized as follows:

- A cell-free scheme for a set of aerial APs (UxNBs) is proposed to manage the severe intercell interference in aerial cellular networks between UxNBs of neighboring cells and terrestrial users.
- We utilize a HAPS as a CPU for backhauling of UxNBs in the sub-THz band. In this paper, instead of a terrestrial CPU, we show how a HAPS can be used as an aerial CPU to process all received signals from all UxNBs. HAPS is an ideal choice to work as a CPU since there is negligible blockage and shadowing for backhaul links between it and the UxNBs which means a reliable LoS link. Hence, we can easily use the upper frequency bands for these links to support the huge bandwidth requirement for backhauling.
- A transceiver scheme at the UxNBs is proposed. At the first time slot of the proposed cell-free scheme, users send their messages to UxNBs at the sub-6 GHz frequency band. Then each UxNB applies match-filtering to align the received signals from users, followed by power allocation among the aligned signals of all users. At the second time slot, at each UxNB, we allocate orthogonal resource blocks (RBs) for each user at the sub-THz band, and forward the filtered signals of all users to the HAPS after analog beamforming.
- A receiver scheme at the HAPS is proposed. At the HAPS, in order to align the received signals for each user from different UxNBs, we perform analog beamforming. Then, we demodulate and decode the message of each user at its own unique RB. Finally, we derive

the achievable rate of the users based on the proposed transceiver and receiver schemes.

- We formulate an optimization problem that maximizes the minimum SINR of users. We find optimum values for two blocks of optimization variables (i.e., the allocated powers for users in each UxNB and the locations of UxNBs), which are solved by the bisection [26] and successive convex approximation (SCA) [27] methods, respectively. Finally, the whole optimization problem is solved by the block coordinate descent (BCD) method [28].

Simulation results demonstrate the superiority of the proposed cell-free scheme compared with the aerial cellular and terrestrial cell-free baseline schemes in urban, suburban, and dense urban environments. Also, simulation results show that utilizing a HAPS as a CPU is useful when the considerable path loss in the sub-THz band between UxNBs and HAPS is compensated for by a high number of antenna elements at the HAPS.

The remainder of this paper is organized as follows. Section II presents the system model. Section III presents the proposed transceiver scheme and the corresponding achievable rate. Section IV provides the formulated optimization problem and its solution for powers and locations of UxNBs. Section V provides simulation results to validate the performance of the proposed scheme. Finally, Section VI concludes the paper.

II. SYSTEM MODEL AND CHANNEL MODEL

A. System Model

The proposed aerial cell-free scheme with HAPS-assisted sub-THz backhauling is shown in Fig. 1. As we can see, M UxNBs are serving K users in the cell-free mode. Each UxNB is assumed to be equipped with a uniform planar array (UPA) with N receive antenna elements positioned on the underside of each UAV working in sub-6 GHz frequency band, and a UPA with G transmit antenna elements on the topside of the UAV working in the sub-THz band. We propose to utilize a HAPS as a CPU to combine the received signals of all UxNBs and decode the messages of all K users. The HAPS is equipped with a UPA with S receive antenna elements working in the sub-THz band. Due to the requirement of K orthogonal RBs for retransmission of the received signals at the UxNBs to the HAPS, we propose to use the sub-THz frequency band for the backhaul links.

In the proposed scheme, the transmission is performed in two time slots. At the first time slot, users send their data to the UxNBs. It should be noted that the severe intercell interference among UAVs of neighboring cells and users is a big problem in the aerial networks. In order to

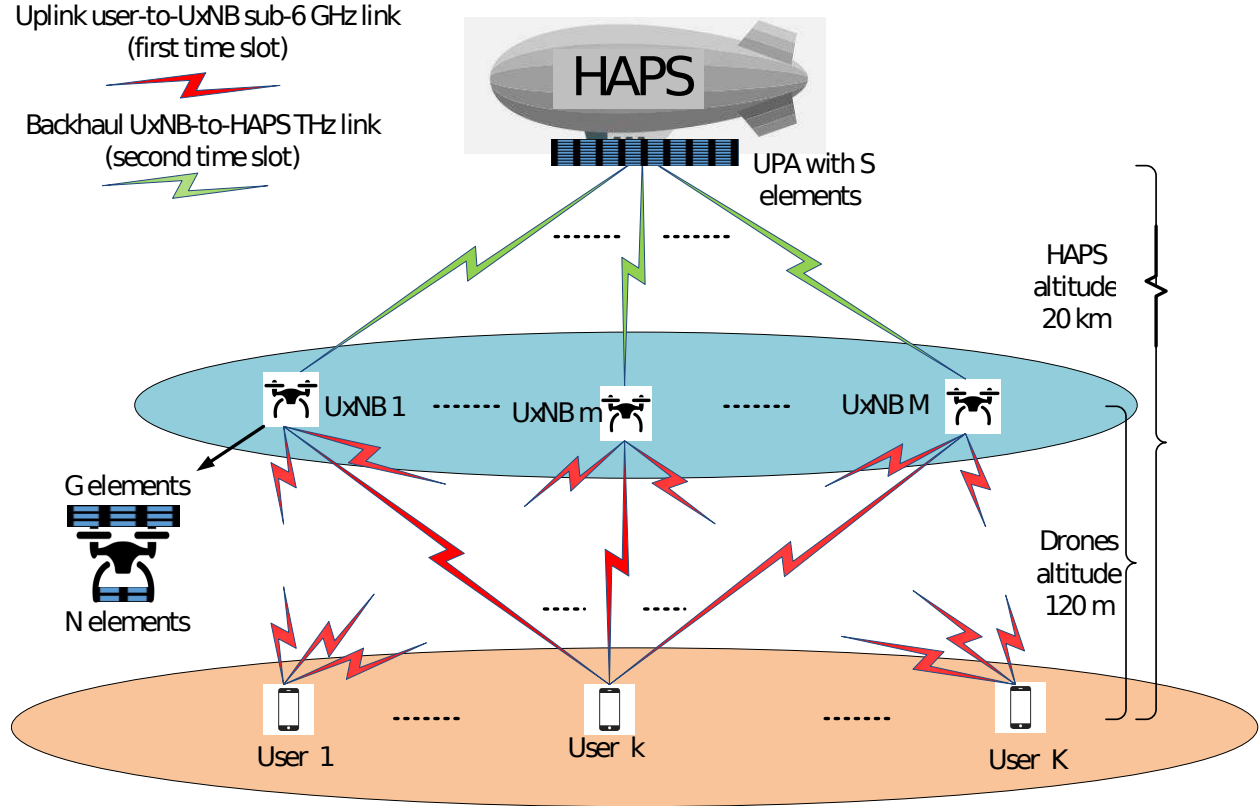


Fig. 1: System model for the proposed cell-free scheme with HAPS-assisted sub-THz backhauling. At the first time slot, users send their messages to UxNBs, and each UxNB applies match filtering for its received signals. At the second time slot, the UxNBs forward each user's filtered signal to the HAPS at orthogonal RBs. Then, HAPS decodes the message of each user as a CPU.

solve this problem, we propose an aerial cell-free scheme where each user is served by multiple UxNBs that establish a strong link with users. At each UxNB, the channel state information (CSI) of the user-to-UxNB links are estimated, and then they are utilized for match-filtering of the received signals. We also divide the total power of each UxNB among the users. Since the instantaneous CSI only needs to be known locally at the UxNBs for the match-filtering scheme, this is a big advantage compared to other schemes, such as zero-forcing, which requires the instantaneous CSI of all links at the CPU [29].

At the second time slot, the UxNBs forward the power-allocated and match-filtered signals to the HAPS. Here, we utilize the sub-THz band for the UxNB to HAPS link, and we allocate orthogonal resource RBs for each user's signal at these backhaul links. This means that in the cell-free scheme, we need K times more bandwidth for backhauling compared to the access

network, which can be satisfied in the sub-THz band. In order to align the received signals for each user from the different UxNBs, we perform analog beamforming based on the steering vectors of the UPA at the HAPS for all UxNBs. Finally, we demodulate and decode the message of each user at its own unique RBs.

B. Channel Model

In our scheme, the channel between user k and antenna element n of UxNB m is indicated by h_{kmn} , which includes both large-scale fading (i.e., path loss and shadowing) and multipath small-scale fading effects. We assume a UPA for the receiver of each UAV with $N = N_w \times N_l$ antenna elements, where N_w and N_l show the number of antenna elements in the width and length of array, respectively. Because there is a LoS link between the users and UAVs, a Ricean distribution is considered for the channel between user k and antenna element $n = (n_w, n_l)$ of UxNB m as follows:

$$h_{kmn} = 10^{-\frac{\text{PL}_{km}}{20}} (\sqrt{P_{km}^{\text{LoS}}} a_{kmn} + \sqrt{P_{km}^{\text{NLoS}}} \mathcal{CN}(0, 1)), \quad (1)$$

where $\mathcal{CN}(0, 1)$ shows a complex normal random variable with the mean value of 0 and the variance (power) of 1. Also,

$$a_{kmn} = \exp(j2\pi(\frac{d_{km}}{\lambda_{\text{sub6}}})) \times \exp(j2\pi(\frac{d_{\text{sub6},w}(n_w - 1) \sin \theta_{km} \cos \phi_{km}}{\lambda_{\text{sub6}}})) \times \exp(j2\pi(\frac{d_{\text{sub6},l}(n_l - 1) \sin \theta_{km} \sin \phi_{km}}{\lambda_{\text{sub6}}})) \quad (2)$$

indicates the phase shift of the LoS link's signal due to distance in which d_{km} shows the distance between user k and UxNB m ; $d_{\text{sub6},w} = \frac{\lambda_{\text{sub6}}}{2}$ ($d_{\text{sub6},l} = \frac{\lambda_{\text{sub6}}}{2}$) is the element spacing along the width (length) of antenna array for each UxNB in sub-6 GHz frequency band f_{sub6} ; $\lambda_{\text{sub6}} = \frac{C}{f_{\text{sub6}}}$ is the wavelength, and $C = 3 \times 10^8$ m/s is the speed of light. The coordinates of each user k and each UAV m are denoted by $(x_{u,k}, y_{u,k}, 0)$ and $(x_{d,m}, y_{d,m}, h_{d,m})$, respectively. Hence the distance between user k and UAV m equals $d_{km} = \sqrt{(x_{u,k} - x_{d,m})^2 + (y_{u,k} - y_{d,m})^2 + (h_{d,m})^2}$. θ_{km} and ϕ_{km} show the elevation and azimuth angles of arrival of the transmitted signal from user k at the UxNB m , respectively. It should be noted that $\mathbf{a}_{km} = [a_{kmn}]_{1 \times N}$ creates the steering vector of the receive antenna array of UAV m for user k . Also, we have $\text{PL}_{km} = P_{km}^{\text{LoS}} \text{PL}_{km}^{\text{LoS}} + P_{km}^{\text{NLoS}} \text{PL}_{km}^{\text{NLoS}}$ in which the LoS and non-LoS (NLoS) path loss of the link between UxNB m and user k are equal to $\text{PL}_{km}^{\text{LoS}} = \text{FSPL}_{km} + \eta_{\text{LoS}}^{\text{dB}}$, and $\text{PL}_{km}^{\text{NLoS}} = \text{FSPL}_{km} + \eta_{\text{NLoS}}^{\text{dB}}$, respectively [30]. In these equations, $\text{FSPL}_{km} = 10 \log(\frac{4\pi f_{\text{sub6}} d_{km}}{C})^2$ shows the free-space path loss (FSPL), and $\eta_{\text{LoS}}^{\text{dB}}$ and $\eta_{\text{NLoS}}^{\text{dB}}$ indicate

the excessive path losses (in dB) affecting the air-to-ground links for LoS and NLoS cases, respectively [31]. $P_{km}^{\text{LoS}} = \frac{1}{1+A \exp(-B(90-\theta_{km})-A)}$ shows the probability of establishing LoS link between user k and UxNB m in which θ_{km} (in degree) shows the elevation angle between user k and UxNB m , and A and B are parameters depending on the environment [30]. $P_{km}^{\text{NLoS}} = 1 - P_{km}^{\text{LoS}}$ shows the probability of establishing a NLoS link between user k and UxNB m .

The large-scale channel power gain for the user k to UxNB m link is equal to

$$\beta_{km}^2 = E\{|h_{kmn}|^2\} = E\{h_{kmn}h_{kmn}^*\} = 10^{-\frac{PL_{km}}{10}} = 10^{-\frac{P_{km}^{\text{LoS}}PL_{km}^{\text{LoS}} + P_{km}^{\text{NLoS}}PL_{km}^{\text{NLoS}}}{10}}. \quad (3)$$

By considering $\beta_0 = (\frac{4\pi f_{\text{sub6}}}{C})^{-2}$ as the channel gain at the reference distance $d_{km} = 1$ m, the large-scale channel power gain can be rewritten as $\beta_{km}^2 = \eta_{km}\beta_0(d_{km})^{-2}$, in which $\eta_{km} = 10^{-\frac{P_{km}^{\text{LoS}}\eta_{\text{LoS}}^{\text{dB}} + P_{km}^{\text{NLoS}}\eta_{\text{NLoS}}^{\text{dB}}}{10}}$ shows the excessive path loss. We consider independent additive white Gaussian noise (AWGN) with the distribution $CN(0, \sigma^2)$ at all antenna elements of all UxNBs. We assume that all of the antenna elements in this paper are omni-directional with antenna gain of 1.

We assume a UPA for the transmitter of each UxNB with $G = G_w \times G_l$ antenna elements in which G_w and G_l show the number of antenna elements along the width and length of the array, respectively. We also assume a UPA at the receiver of the HAPS with a large number of $S = S_w \times S_l$ antenna elements in which S_w and S_l show the number of antenna elements along the width and length of the array, respectively. The channel between the transmit antenna element $g = (g_w, g_l)$ of UxNB m and the receiver antenna element $s = (s_w, s_l)$ of the HAPS, which is in the sub-THz frequency band, is assumed to be LoS, and is equal to

$$g_{mgs} = \gamma_m b_{mg}^* c_{ms}, \quad (4)$$

where

$$\begin{aligned} b_{mg} = & \exp(j2\pi(\frac{d_m}{\lambda_{\text{THz}}})) \times \exp(j2\pi(\frac{d_{\text{THz,d,w}}(g_w - 1) \sin \Theta_m \cos \Phi_m}{\lambda_{\text{THz}}})) \\ & \times \exp(j2\pi(\frac{d_{\text{THz,d,l}}(g_l - 1) \sin \Theta_m \sin \Phi_m}{\lambda_{\text{THz}}})) \end{aligned} \quad (5)$$

indicates the phase shift of the transmitted signal from antenna element g of UxNB m , and where

$$c_{ms} = \exp(j2\pi(\frac{d_{\text{THz,h,w}}(s_w - 1) \sin \Theta_m \cos \Phi_m}{\lambda_{\text{THz}}})) \times \exp(j2\pi(\frac{d_{\text{THz,h,l}}(s_l - 1) \sin \Theta_m \sin \Phi_m}{\lambda_{\text{THz}}})) \quad (6)$$

indicates the phase shift of the received signal from user m at antenna element s of the HAPS. In these equations, d_m indicates the distance between the reference antenna element of UxNB m and the reference antenna element of HAPS; $d_{\text{THz},d,w} = \frac{\lambda_{\text{THz}}}{2}$ ($d_{\text{THz},d,l} = \frac{\lambda_{\text{THz}}}{2}$) is the element spacing along the width (length) of the transmit antenna array at each UxNB in sub-THz frequency band f_{THz} ; $d_{\text{THz},h,w} = \frac{\lambda_{\text{THz}}}{2}$ ($d_{\text{THz},h,l} = \frac{\lambda_{\text{THz}}}{2}$) is the element spacing along the width (length) of the receiver antenna array at the HAPS in the sub-THz frequency band f_{THz} ; and $\lambda_{\text{THz}} = \frac{C}{f_{\text{THz}}}$ is the wavelength. Also, Θ_m and Φ_m show the elevation and azimuth angles of the transmitted signal from UxNB m at the HAPS. It should be noted that $\mathbf{b}_m = [b_{mg}]_{1 \times G}$ creates the steering vector of the transmit antenna array of UxNB m , and $\mathbf{c}_m = [c_{ms}]_{1 \times S}$ creates the steering vector of the receive antenna array of the HAPS transmitted from UxNB m . γ_m^2 shows the path loss between UxNB m and the HAPS. The path loss for sub-THz band is given by $\gamma_m^2 = \rho_m^2 \tau_m = \gamma_0 d_m^{-2} \tau_m$ in which ρ_m^2 is the free space path loss, $\gamma_0 = (\frac{4\pi f_{\text{THz}}}{C})^{-2}$ is the channel gain at the reference distance $d_m = 1$ m, and $\tau_m = 10^{-Kh_m^e/10}$ shows the transmittance of the medium following the Beer-Lambert law in which K (in dB/km) is the absorption coefficient of the medium, which is a function of frequency and altitude [23]. Also, $h_m^e = \frac{h^e}{\sin \Theta_m} = \frac{h^e d_m}{h_{\text{HAPS}} - h_{d,m}}$ shows the effective height of a medium for UxNB m in which h_e indicates the effective height for a UxNB that is located in the nadir of the HAPS [32].

It should be noted that the absorbed part of the sub-THz signal by the medium due to the molecule absorption (i.e., $1 - \tau_m$ percent of the transmitted signal from UxNB m) will be re-emitted by the molecules with some delay, and hence we consider this re-emitted signal as re-emission interference in our rate derivations [33]. We assume that this delayed re-emitted signal has a random phase as $\exp(j\omega)$ in which ω is a random variable with uniform distribution such that $U(0, 2\pi)$. We consider independent AWGN with the distribution $CN(0, \sigma_H^2)$ at all antenna elements of the HAPS.

III. PROPOSED TRANSCEIVER SCHEME AT UXNBs AND HAPS

We can see the proposed transceiver scheme at UxNB m in Fig. 2. At the first time slot of the proposed scheme, each user transmits its message to the UxNBs. The transmitted signal by user k is shown by $\sqrt{P_k} s_k$ in which P_k (for $k \in \{1, 2, \dots, K\}$) indicates the maximum transmit power at each user k , and s_k ($E\{|s_k|^2\} = 1$) is the transmitted symbol from user k . The received signal at the antenna element n of UxNB m 's UPA equals $y_{mn} = \sum_{k=1}^K h_{kmn} \sqrt{P_k} s_k + z_m$ in which z_m is the AWGN noise at the receiver of UxNB m . After receiving y_{mn} at the antenna element

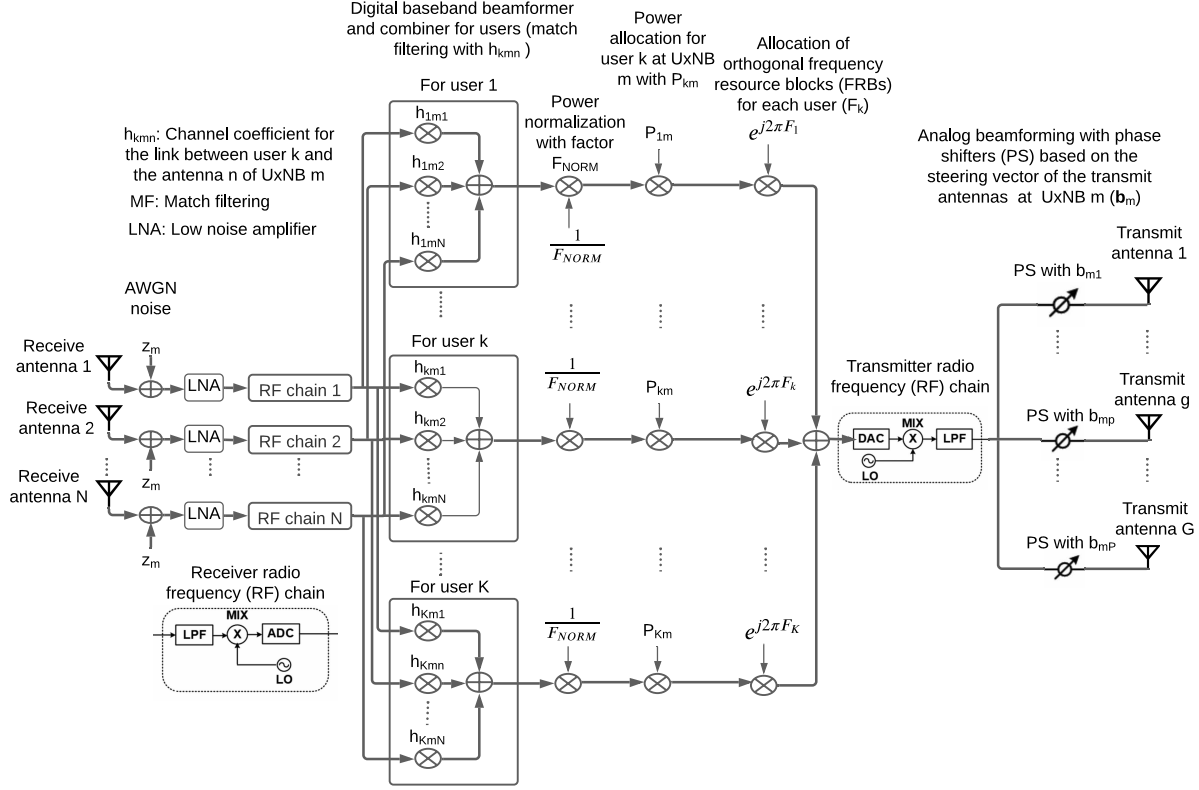


Fig. 2: The proposed transceiver scheme at UxNB m .

n of UxNB m , the low noise amplifier (LNA) block amplifies this signal, and then the radio frequency (RF) chains downconvert the signal to a baseband one and convert the analog signal to a digital signal. Next, at the digital baseband beamforming block for each user and according to the estimated CSI for the channel between user k and antenna element n of UxNB m (i.e., h_{kmn}), we perform match-filtering such that $y_{kmn}^{\text{MF}} = y_{mn} \times \frac{h_{kmn}^*}{|h_{kmn}|}$, and we combine these match-filtered signals to arrive at $y_{km}^{\text{COMB}} = \sum_{n=1}^N y_{kmn}^{\text{MF}}$ [34]. It should be noted that x^* indicates the conjugate of x . Then, we allocate the power P_{km} for each user so that we must have $\sum_{k=1}^K P_{km} \leq P_m$ for each UxNB m , in which P_m shows the total power at UxNB m . We now need to normalize the signal for each user before power allocation such that $y_{km}^{\text{NORM}} = \frac{y_{km}^{\text{COMB}}}{|y_{km}^{\text{COMB}}|}$ in which $|x|$ shows the absolute value of x . Therefore, the signal for each user k at UxNB m after power normalization and power allocation will be $y_{km} = \sqrt{P_{km}} y_{km}^{\text{NORM}}$. In order to transmit these K signals to the HAPS, we allocate orthogonal frequency RBs for each of them to avoid interference among the filtered signals of different users. It should be noted that the same frequency RBs are allocated

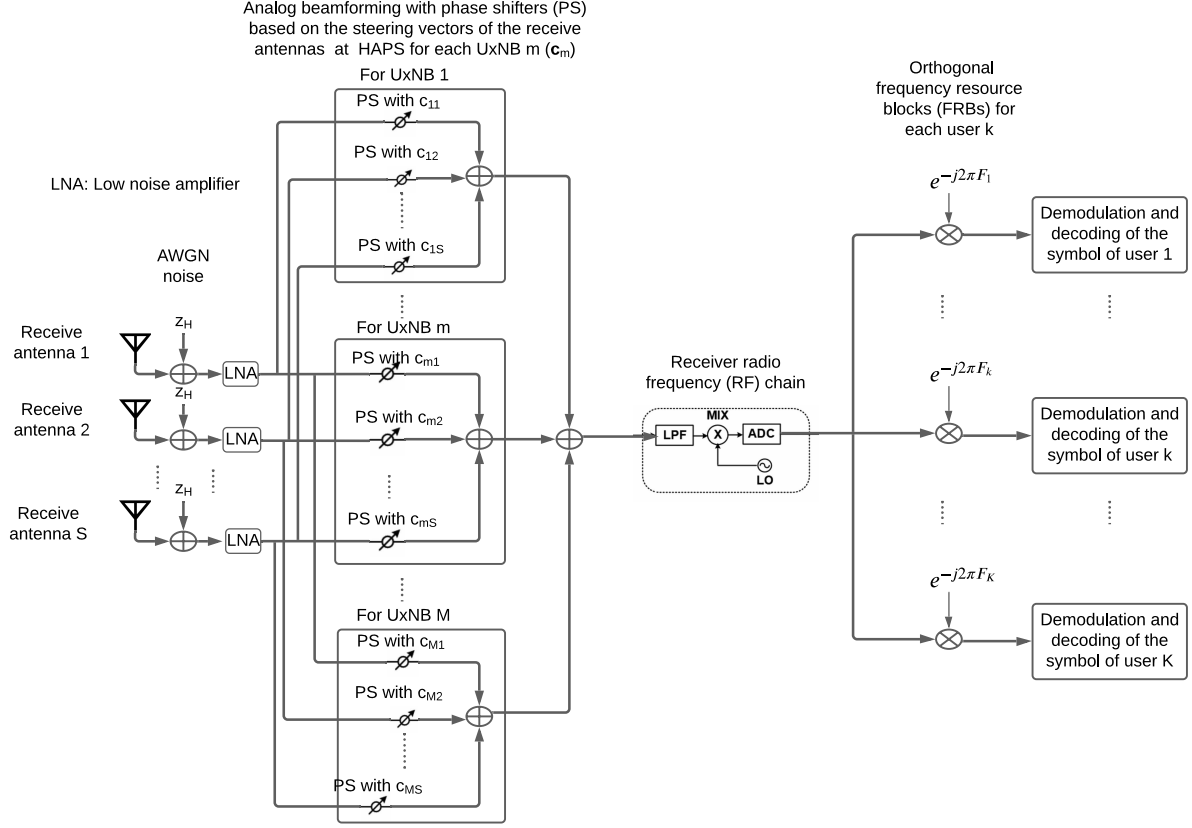


Fig. 3: The proposed receiver scheme at HAPS for decoding of the message of users.

for each user at different UxNBs, which means that we need K RBs at the second time slot of the proposed scheme in total. These RBs can be easily provided at the sub-THz frequency band. The digital signal for users is converted to an analog one and upconverted to the sub-THz frequency band utilizing an RF chain. In order to transmit signals from each UxNB to the HAPS, we utilize only one RF chain because we apply fully analog beamforming. We perform the analog beamforming with phase shifter (PSs) to direct the transmitted signal from each UxNB to the HAPS. This is done by multiplying the signal by b_{mg} in (5) for each transmit antenna element g of each UxNB m . It should be noted that the transmitted signal for user k from antenna element g of UxNB m equals $b_{mg}y_{km}$.

The transmitted signal from each UxNB m will be received at each antenna element s of the HAPS after passing through the channel between them (i.e., g_{mps}). Hence, the received signal

at RB k and antenna element s of the HAPS is given by

$$\begin{aligned} y_s^k &= \sum_{m=1}^M \sum_{g=1}^G g_{mgs} b_{mg} y_{km} + z_H \\ &= \sum_{m=1}^M \sum_{g=1}^G c_{ms} \gamma_m b_{mg} b_{mg}^* y_{km} + z_H = G \sum_{m=1}^M c_{ms} \gamma_m y_{km} + z_H \end{aligned} \quad (7)$$

in which z_H is the AWGN noise at each receive antenna element of the HAPS. Superscript k shows the received signal at RB k . We can see the proposed receiver scheme at HAPS for decoding the message of users in Fig. 3. As one can see, first the LNA blocks amplify the received signals. In the proposed receiver scheme at the HAPS, we perform analog beamforming with PSs to align the received signals from each UxNB m at the receive antenna elements of the HAPS. To do this, we multiply the signal y_s^k by conjugate of the steering vector of the receive antenna elements at HAPS for each UxNB m , i.e., c_m^* in (6), and then combine these signals as follows:

$$y^k = \sum_{m=1}^M \sum_{s=1}^S c_{ms}^* y_s^k. \quad (8)$$

Next, an RF chain downconverts the signal to a baseband one, and converts the analog signal to a digital signal. In order to receive and decode signals of all UxNBs at the HAPS, we utilize only one RF chain since we apply fully analog beamforming. As mentioned above, we allocate orthogonal RBs for each user at the UxNB-to-HAPS sub-THz links, and for this reason the received signal for each user can be separately achieved at the HAPS. Finally, utilizing this signal y^k , we demodulate and decode the symbol of each user k .

Now, in the following proposition, we derive the SINR of each user utilizing the signal y^k .

Proposition 1. *The achievable rate of the user k in the proposed aerial cell-free scheme with HAPS-assisted backhauling in the THz band is given by*

$$R_k = \log_2(1 + \text{SINR}_k) \quad (9)$$

in which

$$\text{SINR}_k = \frac{MG^2 N S P_k (\sum_{m=1}^M \gamma_m \sqrt{P_{km}} \beta_{km})^2}{MG^2 \sum_{m=1}^M \rho_m^2 P_{km} \sum_{k'=1}^K \beta_{k'm}^2 P_{k'} + MG^2 \sum_{m=1}^M \rho_m^2 P_{km} \sigma^2 + \sigma_H^2 (\sum_{m=1}^M \sum_{k'=1}^K \beta_{k'm}^2 P_{k'} + M \sigma^2)}. \quad (10)$$

Proof. Please see Appendix A. □

In terms of 5G terminology, the UxNB nodes in the system model in Fig. 1 have the same functionality with distributed units (DUs), and the HAPS has the same functionality with a

centralized unit (CU) [35]. In the study item for the new radio access technology, different functional splits between the CU and the DU have been studied [36]. Split option 7 itself has three variants, depending on what aspects of the physical layer processing are performed in the DU and CU. Indeed, in option 7, the lower physical layer functions and RF circuits are located in the DU(s), and the upper protocol layers including the upper physical layer functions reside in the CU. Our proposed transceiver scheme at each UxNB in Fig. 2 resides between the option 7-2 and option 7-3 functional split between the CU and DU. This is because we do not demodulate and decode the received signals at DU, and we simply apply match-filtering and power allocation for the received signals. Then, we upconvert the signals to the sub-THz band and transmit them to the CU (HAPS) in orthogonal RBs. It should be noted that all of these functions happen in layer 1 (physical layer). We should add that, in general, the links between the DUs and CU are assumed to be perfect when connected with a fiber link. However, in our proposed transceiver scheme for the uplink, at each DU, we have a transmission part to prepare and design beamformer for the signals, and forward them to the CU wirelessly. This is one of the main differences between our work and terrestrial cell-free schemes in the literature.

IV. OPTIMIZATION PROBLEM

In this section, we formulate an optimization problem that maximizes the minimum SINR of users. We find the optimum allocated powers for users in each UxNB (i.e., $\mathbf{P} = [P_{km}]_{K \times M}$) and the optimum locations of UxNBs (i.e., $\mathbf{x} = [x_{d,m}]_{1 \times M}$ and $\mathbf{y} = [y_{d,m}]_{1 \times M}$) We can write the optimization problem as follows:

$$(P): \quad \max_{\mathbf{P}, \mathbf{x}, \mathbf{y}} \quad \min_k \quad \text{SINR}_k \quad (11)$$

$$\text{s.t.} \quad \sum_{k=1}^K P_{km} \leq P_m, \quad \forall m, \quad (12)$$

$$P_{km} > 0, \quad \forall k, \forall m, \quad (13)$$

$$x_{\min} \leq x_{d,m} \leq x_{\max}, \quad y_{\min} \leq y_{d,m} \leq y_{\max}, \quad \forall m, \quad (14)$$

where constraint (12) shows the maximum total power constraint at each UxNB m , and constraint (14) indicates the horizontal range of the UxNBs' flight. Problem (P) is a non-convex optimization problem due to its objective function, which is not concave with respect to variables \mathbf{P} , \mathbf{x} and

y. In order to solve this problem, first, based on the BCD method [28], we split the optimization problem into two sub-problems. In the first sub-problem, we solve the problem (P) for the case where locations of the UxNBs (i.e., x and y) are given, and in the second optimization sub-problem, the power allocation coefficients P are assumed to be given. It should be noted that the power allocation problem can be equivalent to the case where we do not have control of the locations of the UxNBs, and they are non-dedicated aerial users that perform their own missions, and we utilize them as APs of the cell-free scheme as well. Both power allocation and deployment sub-problems are still non-convex, and we solve them by means of the bisection and SCA methods in the following two sub-sections, respectively.

A. Power Allocation Sub-Problem

If we fix the locations of the UxNBs in (P), we will have the power allocation sub-problem as follows:

$$(P1): \max_{\mathbf{P}} \min_k \text{SINR}_k \quad (15)$$

$$\text{s.t.} \quad \sum_{k=1}^K P_{km} \leq P_m, \quad \forall m, \quad (16)$$

$$P_{km} > 0, \quad \forall k, \forall m. \quad (17)$$

This problem is still non-convex with respect to power allocation coefficients P .

Proposition 2. *The optimization problem (P1) is a quasi-concave optimization problem.*

Proof. Please see Appendix B. □

Since problem (P1) is a quasi-concave optimization problem, its optimal solution can be found efficiently by the bisection method [26]. To do this, we rewrite the problem (P1) by adding slack variable η as follows:

$$(P2): \max_{\mathbf{P}, \eta} \eta \quad (18)$$

$$\text{s.t.} \quad \text{SINR}_k \geq \eta, \quad \forall k \quad (19)$$

$$\sum_{k=1}^K P_{km} \leq P_m, \quad \forall m, \quad (20)$$

$$P_{km} > 0, \eta > 0, \quad \forall k, \forall m. \quad (21)$$

It can be easily proven that (P2) is equivalent to (P1). For this, it should be noted that at the optimal solution for (P2), we must have $\eta = \min(\text{SINR}_1, \dots, \text{SINR}_K) = \text{SINR}_1 = \dots = \text{SINR}_K$, which is the same with the optimal solution for (P1), and hence we can continue with (P2). By performing the variable change $\mathbf{T} = [P_{km}^2]_{K \times M}$, for any given value of η , problem (P2) will be a convex feasibility problem that can be solved optimally by convex optimization techniques, such as the interior-point method. The summary of this bisection method is shown in Algorithm 1.

Algorithm 1 Bisection method for solving the power allocation problem (P1) with the given locations of UxNBs.

- 1: Initialize the values of η_{\min} and η_{\max} , where η_{\min} and η_{\max} show a range for the minimum SINR of users. Choose a tolerance $\epsilon > 0$.
- 2: **repeat**
- 3: Set $\eta = \frac{\eta_{\min} + \eta_{\max}}{2}$ and solve the convex feasibility problem (P2) by the interior-point method.
- 4: If the problem (P2) is feasible, set $\eta_{\min} = \eta$; else set $\eta_{\max} = \eta$.
- 5: **until** $\eta_{\max} - \eta_{\min} < \epsilon$.

B. UxNBs Placement Sub-Problem

For a given allocated powers in (P), we will have the following placement sub-problem:

$$(P3): \quad \max_{\mathbf{x}, \mathbf{y}} \quad \min_k \quad \text{SINR}_k \quad (22)$$

$$\text{s.t.} \quad x_{\min} \leq x_{d,m} \leq x_{\max}, \quad y_{\min} \leq y_{d,m} \leq y_{\max}, \quad \forall m. \quad (23)$$

This problem is still non-convex with respect to variables \mathbf{x} and \mathbf{y} . By substituting the SINR formula from (10) and introducing three slack variables η , $\mathbf{t} = [t_k]_{1 \times K}$, and $\boldsymbol{\beta} = [\beta_{km}]_{K \times M}$, (P3) can be rewritten as follows:

$$(P4): \max_{\mathbf{x}, \mathbf{y}, \eta, \mathbf{t}, \boldsymbol{\beta}} \eta \quad (24)$$

$$\text{s.t.} \quad \frac{\sqrt{MG^2NSP_k}(\sum_{m=1}^M \gamma_m \sqrt{P_{km}} \beta_{km})}{t_k} \geq \sqrt{\eta}, \forall k \quad (25)$$

$$t_k \geq \sqrt{MG^2 \sum_{m=1}^M \rho_m^2 P_{km} \sum_{k'=1}^K \beta_{k'm}^2 P_{k'} + MG^2 \sum_{m=1}^M \rho_m^2 P_{km} \sigma^2 + \sigma_H^2 (\sum_{m=1}^M \sum_{k'=1}^K \beta_{k'm}^2 P_{k'} + M \sigma^2)}, \forall k \quad (26)$$

$$\beta_{km}^{-1} \geq 10^{\frac{P_{km}^{\text{LoS}} \eta_{\text{LoS}}^{\text{dB}} + P_{km}^{\text{NLoS}} \eta_{\text{NLoS}}^{\text{dB}}}{20}} \beta_0^{-\frac{1}{2}} \sqrt{(x_{u,k} - x_{d,m})^2 + (y_{u,k} - y_{d,m})^2 + (h_{d,m})^2}, \forall k, \forall m \quad (27)$$

$$x_{\min} \leq x_{d,m} \leq x_{\max}, \quad y_{\min} \leq y_{d,m} \leq y_{\max}, \quad \forall m \quad (28)$$

$$\eta > 0, t_k > 0, \beta_{km} > 0, \forall k, \forall m. \quad (29)$$

It can be easily proven that (P4) is equivalent to (P3). As we can see, constraint (26) is in the form of a norm function of variable $\boldsymbol{\beta}$ less than an affine function of variable \mathbf{t} , and hence it is a convex set. However, this problem is still non-convex due to constraints (25) and (27). To address constraint (25), we perform a variable change such that $\eta = \zeta^4$. Hence, for the optimization problem (P4) we can write the following:

$$(P5): \max_{\mathbf{x}, \mathbf{y}, \zeta, \mathbf{t}, \boldsymbol{\beta}} \zeta \quad (30)$$

$$\text{s.t.} \quad \frac{1}{t_k} \geq \frac{\zeta^2}{\sqrt{MG^2NSP_k}(\sum_{m=1}^M \gamma_m \sqrt{P_{km}} \beta_{km})}, \forall k \quad (31)$$

$$(26), (27), (28), (29). \quad (32)$$

One can see that the right-hand side of (31) is in the form of a quadratic function of variable ζ over an affine function of variable $\boldsymbol{\beta}$, which is known to be a convex function when its denominator is positive [27]. Also, the right-hand side of (27) is in the form of a norm function of variables \mathbf{x} and \mathbf{y} , and so it is convex. However, the left-hand side of the constraints (27) and (31) (i.e., $\frac{1}{\beta_{km}}$ and $\frac{1}{t_k}$) are not in the form of a concave function. In order to manage these non-concave terms, we propose an iterative scheme based on the SCA method [37]. In this method, the original non-convex problem is optimized by solving convex approximations of the original problem iteratively around an initial point until convergence. These approximations must lead to non-decreasing values for the objective function with the increase of the iteration number l

in order to guarantee the convergence of the SCA method. We know that the first-order Taylor series expansion of a convex function $f(z)$ provides a global lower-bound for that function, i.e., $f(z) \geq f(z_0) + \nabla f(z_0)^T(z - z_0)$. Given that the left-hand side of the constraints (27) and (31) are in the form of a convex function, we can approximate them at each iteration $l + 1$ by their first-order Taylor series expansion around the solution of the previous iteration l . Therefore, at the iteration $(l + 1)$, we replace the left-hand side of the constraints (27) and (31) with the expressions $-\frac{1}{(\beta_{km}^l)^2}(\beta_{km} - \beta_{km}^l) + \frac{1}{\beta_{km}^l}$ and $-\frac{1}{(t_k^l)^2}(t_k - t_k^l) + \frac{1}{t_k^l}$, respectively. It is clear that these functions are affine functions with respect to variables t and β . Now, by replacing these approximations in (P5), the optimization problem at the iteration $l + 1$ of the SCA method around the initial points t^l and β^l is given by

$$(P6): \max_{\mathbf{x}, \mathbf{y}, \zeta, \mathbf{t}, \boldsymbol{\beta}} \zeta \quad (33)$$

$$\text{s.t.} \quad -\frac{1}{(t_k^l)^2}(t_k - t_k^l) + \frac{1}{t_k^l} \geq \frac{\zeta^2}{\sqrt{MG^2NSP_k}(\sum_{m=1}^M \gamma_m \sqrt{P_{km}} \beta_{km})}, \forall k \quad (34)$$

$$-\frac{1}{(\beta_{km}^l)^2}(\beta_{km} - \beta_{km}^l) + \frac{1}{\beta_{km}^l} \geq 10^{\frac{P_{km}^{\text{LoS}} \eta_{\text{LoS}}^{\text{dB}} + P_{km}^{\text{NLoS}} \eta_{\text{NLoS}}^{\text{dB}}}{20}} \beta_0^{-\frac{1}{2}} \sqrt{(x_{u,k} - x_{d,m})^2 + (y_{u,k} - y_{d,m})^2 + (h_{d,m})^2}, \forall k, \forall m \quad (35)$$

$$(26), (28), (29). \quad (36)$$

This optimization problem is convex since all of the constraints are in the form of a convex function of variables less than a concave function of variables. This problem can be efficiently solved by convex optimization techniques, such as the interior-point method. The optimum value for the objective function of (P3) can be derived from $\eta = \zeta^{\frac{1}{4}}$. One can see the summary of the proposed iterative method for solving (P3) in Algorithm 2. Now, since the objective function of (P6) is non-decreasing over iterations and is globally upper-bounded by the optimal value of (P3), the proposed sub-optimal algorithm is guaranteed to converge. Also, since each iteration of Algorithm 2 only requires solving a convex problem, the overall complexity of Algorithm 2 is polynomial in the worst scenario.

C. Iterative Algorithm for Joint Power Allocation and Placements of UxNBs

In this subsection, we apply the BCD method [28] to solve the original problem (P), and find optimized values for power allocation and location variables. For this, we solve the placement of UxNBs and power allocation sub-problems alternately. At each iteration, after initialization of

Algorithm 2 Iterative SCA method for solving the placement optimization problem (P3) with the given power allocation.

- 1: Initialize the locations of UxNBs, i.e., \mathbf{x}^l and \mathbf{y}^l , and let $l = 0$.
- 2: **repeat**
- 3: Solve the convex problem (P6) by the interior-point method and find the optimum values for \mathbf{x} and \mathbf{y} .
- 4: Update $l = l + 1$, and set $\mathbf{x}^l = \mathbf{x}$ and $\mathbf{y}^l = \mathbf{y}$.
- 5: **until** convergence or a maximum number of iterations is reached.

power and location, we optimize the location variables utilizing Algorithm 2. Then, using these locations, we find the optimum power allocation with the aid of Algorithm 1. These powers are used as initial values in the next iterations. The associated algorithm is summarized in Algorithm 3.

It should be noted that the optimal value of the original problem (P) is a global upper-bound for the optimal values of the sub-problems (P1) and (P3), and hence it is also an upper-bound for the optimal value of Algorithm 3. Also, since Algorithm 3 performs Algorithm 1 and Algorithm 2 alternately, the objective value of Algorithm 3 is non-decreasing with iteration number l . As a result, the proposed sub-optimal method at Algorithm 3 is guaranteed to converge. Also, It should be noted that since each iteration of Algorithm 3 only requires solving convex problems, the overall complexity of Algorithm 3 is polynomial in the worst scenario.

V. NUMERICAL RESULTS

In this section, numerical results are provided in order to show the performance gain of the proposed scheme. The following default parameters are applied in the simulations except that we specify different values for them. For the carrier frequency of the first and second hops, we assume $f_{\text{sub}6} = 2$ GHz and $f_{\text{THz}} = 120$ GHz, respectively. The communication bandwidth is assumed to be $\text{BW} = 1$ MHz, and the noise power spectral density is $N_0 = -174$ dBm/Hz. We assume that all users are uniformly distributed over a square area with a length of 1000 meters. Also, we assume that the HAPS is deployed in the middle of this square area. The default values for the number of users, number of UxNBs, number of antenna elements in the receive UPA of each UxNB, number of antenna elements in the transmit UPA of each UxNB, and number of antenna elements in the receive UPA of the HAPS are equal to $K = 16$, $M = 16$, $N = 4$, $G = 9$,

Algorithm 3 Iterative algorithm based on BCD to jointly find the power allocation and placement of UxNBs in problem P.

- 1: Initialize power allocation variables \mathbf{P}^l , and UxNB locations \mathbf{x}^l and \mathbf{y}^l , and let $l = 0$.
- 2: **repeat**
- 3: Solve the non-convex placement problem (P6) with the given powers \mathbf{P}^l and initial locations \mathbf{x}^l and \mathbf{y}^l by the SCA method in Algorithm 2 and find the optimum values for \mathbf{x} and \mathbf{y} .
- 4: Solve the quasi-convex problem (P2) with the given UxNBs locations \mathbf{x} and \mathbf{y} by the bi-section method in Algorithm 1, and find the optimal values for \mathbf{P} .
- 5: Update $l = l + 1$; and set $\mathbf{x}^l = \mathbf{x}$, $\mathbf{y}^l = \mathbf{y}$, and $\mathbf{P}^l = \mathbf{P}$.
- 6: **until** convergence or a maximum number of iterations is reached.

and $S = 400$, respectively. We set the maximum transmit power at each user and each UxNB as $P_k = 0.2$ W, $\forall k$ and $P_m = 25$ dBm, $\forall m$, respectively. We assume that all users send their signals with their maximum power. Considering an urban area, the excessive path loss affecting the air-to-ground links in LoS and NLoS cases is assumed to be $\eta_{\text{LoS}}^{\text{dB}} = 1$ dB and $\eta_{\text{NLoS}}^{\text{dB}} = 20$ dB, respectively [31]. Also, for the urban area, we have $A = 9.61$ and $B = 0.16$. The absorption coefficient of the sub-THz medium for $f_{\text{THz}} = 120$ GHz is equal to $K = 0.5$ dB/km and the effective height is given by $h^e = 1.6$ km [14]. We assume an initial uniform square placement for M UAVs, and a fixed flight height $h_{d,m} = 120$ m, $\forall m$ for all of the UAVs. In Algorithm 1, we set initial values as $\eta_{\min} = 0$ and $\eta_{\max} = 1500$, and also the tolerance value as $\epsilon = 0.01$. We also consider the HAPS altitude as 20 km.

In the simulation figures, the proposed scheme, called **aerial cell-free scheme**, is compared with two baseline schemes. **1) Aerial cellular scheme** in which each terrestrial user is served by only one UxNB. In this baseline method, all of the other parameters and channel models are the same as the proposed scheme. The backhauling of this baseline scheme, same as the proposed scheme, is performed through the HAPS in the sub-THz band. **2) Terrestrial cell-free scheme** in which each terrestrial user is served by multiple terrestrial access points, and a perfect backhaul with fiber links is assumed to connect the APs and CPU. In this baseline scheme, the Raleigh fading model is considered for the channels between the users and APs. Also, in order to have a fair comparison, the number of the receiver antenna elements at terrestrial APs is assumed to be

the same as the number of the receiver antenna elements at UxNBs (i.e., N) in aerial schemes. The match-filtering method is applied in each AP at both baseline schemes to align the received signals.

Fig. 4 shows the achievable minimum rate per user versus the total power of each UxNB ($P_1 = \dots = P_M$) for the aerial and terrestrial BSs with cell-free and cellular schemes. We can see that the proposed aerial cell-free scheme has a better performance compared with the aerial cellular scheme for both values of $S = 100$ and $S = 400$. Indeed, due to the severe intercell interference from other users in the neighboring cells in the aerial cellular scheme, our proposed scheme has much better performance than this baseline scheme. Also in this figure, we can see that the terrestrial cell-free baseline scheme has a constant value by increasing APs powers since we considered a perfect backhaul for this scheme. Our proposed scheme has much better performance than this baseline scheme as well. This is because in the terrestrial cell-free scheme, due to a high path loss and shadowing, the link between a user and far access points can be very weak, and hence working in cell-free mode is not useful. However, in the proposed aerial cell-free scheme, since there is a strong LoS link between the users and UxNBs, the signal of each user is received at multiple UxNBs, and so the cell-free scheme is useful for the proposed system model.

Fig. 5 shows the achievable minimum rate per user versus the number of UxNBs (M) for the aerial and terrestrial BSs with cell-free and cellular schemes. We can see that the proposed aerial cell-free scheme outperforms the aerial cellular scheme for both values of $S = 100$ and $S = 400$. Further, we can see that by increasing M , the improvement in the performance of aerial schemes is much more than the terrestrial scheme, and this is because of a higher probability of establishing LoS links between UxNBs and users for a larger M in aerial schemes. Finally, it is also shown that the superiority of the aerial cell-free scheme over aerial cellular scheme increases by M which is due to a higher intercell interference for the cellular scheme at a higher M .

Fig. 6 indicates the achievable minimum rate per user versus the number of users (K) for the aerial and terrestrial BSs with cell-free and cellular schemes. We set the parameter values as $P_m = 25$ dBm, $\forall m$, $M = 16$, $N = 4$, and $G = 9$. As we can see, by increasing K , the performance of all schemes decreases. Also, we can see that the proposed aerial cell-free scheme performs better than both the aerial cellular and terrestrial cell-free baseline schemes due to the LoS link between the users and UxNBs. Further, by increasing S , the performance

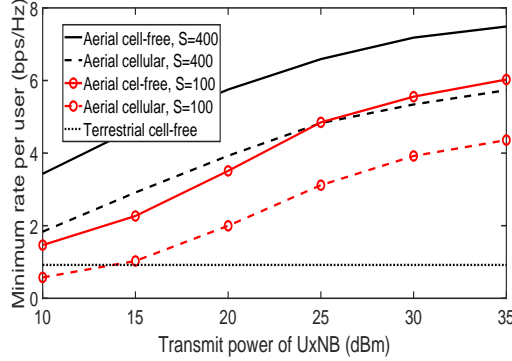


Fig. 4: The achievable minimum rate per user versus the total power of each UxNB ($P_1 = \dots = P_M$) for the aerial and terrestrial BSs with cell-free and cellular schemes. We set $K = 16$, $M = 16$, $N = 4$, and $G = 9$.

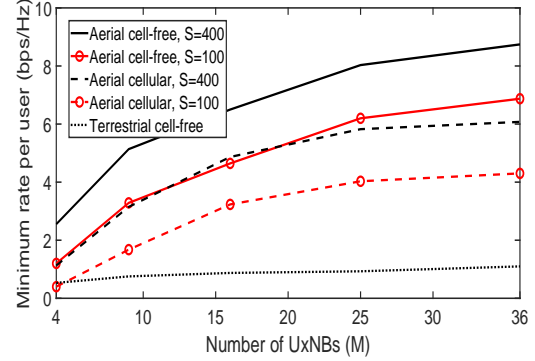


Fig. 5: The achievable minimum rate per user versus the number of UxNBs (M) for the aerial and terrestrial BSs with cell-free and cellular schemes. We set $P_m = 25$ dBm, $\forall m$, $K = 16$, $N = 4$, and $G = 9$.

of the aerial schemes improve, which means that by increasing S we can serve more users for a given minimum rate per user.

Fig. 7 indicates the achievable minimum rate per user versus the number of HAPS antenna elements (S). One can see that when the number of HAPS antenna elements is low, the performance of the aerial and terrestrial schemes are close. For example, when $S = 16$, the terrestrial cell-free scheme performs better than the aerial cellular scheme, and its performance is comparable to the proposed aerial cell-free scheme. However, when the number of HAPS antenna elements is high, both aerial schemes have significant performance gain over the terrestrial cell-free scheme. This figure shows that utilizing a HAPS as a CPU is useful when the enormous path loss between the UxNBs and the HAPS in the sub-THz band is compensated for by a high number of antenna elements at the HAPS.

Fig. 8 shows the CDF of the minimum rate per user ($R_1 = \dots = R_K$) for the aerial and terrestrial BSs with cell-free and cellular schemes. We can see that the proposed aerial cell-free scheme has a better performance compared with both the aerial cellular and terrestrial cell-free baseline schemes for both values of $M = 8$ and $M = 16$. We can also see that the aerial cellular scheme outperforms the terrestrial cell-free scheme, and this is due to the LoS links that are established between users and UxNBs in the aerial networks. Further, we can see that the variance of the minimum achievable rate per user for the cell-free scheme is less than the cellular one, and we can observe that increasing the number of UxNBs reduces the variance of

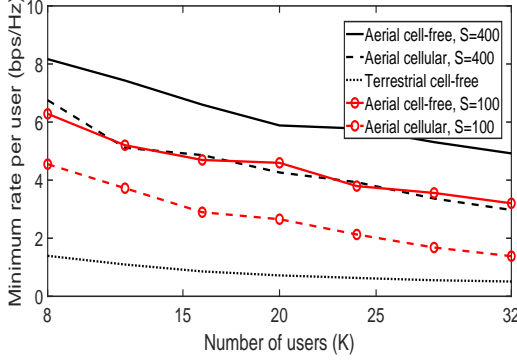


Fig. 6: The achievable minimum rate per user versus number of users (K) for the aerial and terrestrial BSs with cell-free and cellular schemes. We set $P_m = 25$ dBm, $\forall m$, $M = 16$, $N = 4$, and $G = 9$.

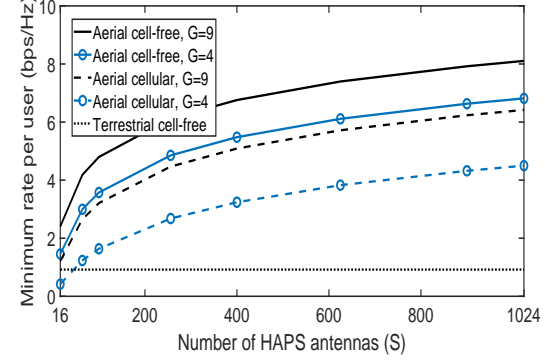


Fig. 7: The achievable minimum rate per user versus number of HAPS antenna elements (S) for the cell-free and cellular schemes. We set $P_m = 25$ dBm, $\forall m$, $M = 16$, $K = 16$, $N = 4$, and $G = 4, 9$.

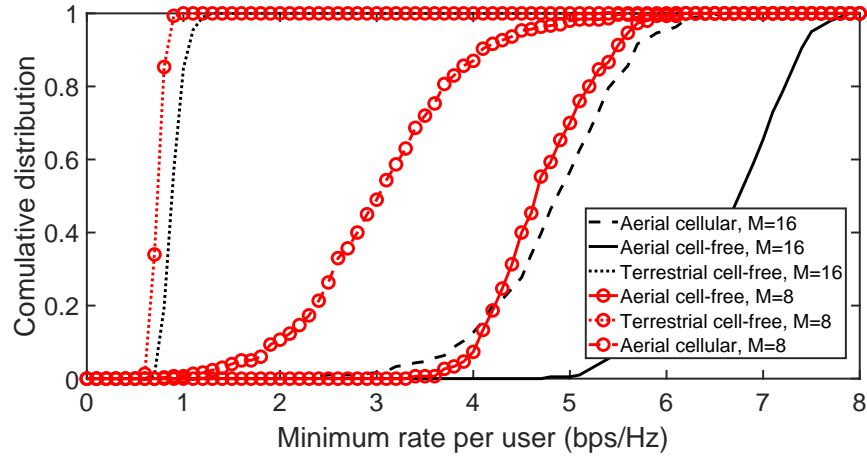


Fig. 8: The CDF of the minimum rate per user ($R_1 = \dots = R_K$) for the aerial and terrestrial BSs with cell-free and cellular schemes. We set $P_m = 25$ dBm, $\forall m$, $K = 16$, $S = 400$, $N = 4$, and $G = 9$.

the minimum achievable rate per user for both aerial cell-free and aerial cellular schemes.

Fig. 9 indicates the achievable minimum rate per user in the proposed cell-free scheme versus the number of UxNBs (M) for the cases where the locations of UxNBs and/or allocated power for each user at each UxNB are optimized. In this figure, we consider heuristic solutions for power allocation and locations of UxNB, and compare them with the optimized values. In the heuristic solution for power allocation, we assume that all of the power of each UxNB is equally divided among users. In the heuristic solution for locations of UxNBs, we uniformly deploy them

over a square area with equal distance with each other.¹ We can see that when we use heuristic solutions for both power allocation and locations, the worst performance is achieved. Also, we can see that the optimization of power with Algorithm 1 improves the performance of the proposed scheme. This figure indicates that the performance of the case that both power and location are jointly optimized with Algorithm 3 is the same as the performance of the case where the location is optimized with Algorithm 2 and the heuristic solution is utilized for power allocation. This means that when the locations of UxNBs are optimized, equal power allocation is the optimal solution for power. This is because by optimizing the locations of the UxNBs, all users reach to equal rates, and hence the optimal policy for power allocation is to divide the total power equally among the users. It should be noted that in the optimal point of our max-min optimization problem, all users must have the same rates.

Fig. 10 shows the achievable minimum rate per user in the proposed cell-free scheme versus the total power of each UxNB ($P_1 = \dots = P_M$) for the cases where the locations of UxNBs and/or allocated power for each user at each UxNB are optimized. We set the parameter values as $K = 16$, $M = 16$, $S = 400$, $N = 4$, and $G = 9$. We consider the same heuristic solutions with Fig. 9 for power allocation and locations of UxNBs. We can see that optimizing power is more useful for lower transmit powers because there is enough power resources at higher transmit powers for managing the fairness among users. Also, as in Fig. 9, we can see that when the locations of UxNBs are optimized, equal power allocation is the optimal solution for power.

Fig. 11 shows the achievable minimum rate per user versus the total power of each UxNB ($P_1 = \dots = P_M$) in aerial schemes for three urban, suburban, and dense urban environments. According to [31], the excessive path losses affecting the air-to-ground links in LoS and NLoS cases, i.e., $(\eta_{\text{LoS}}^{\text{dB}}, \eta_{\text{NLoS}}^{\text{dB}})$, are equal to $(0.1, 21)$, $(1, 20)$, and $(1.6, 23)$ for suburban, urban, and dense urban environments, respectively. Also, parameters (A, B) are equal to $(4.88, 0.43)$, $(9.61, 0.16)$, and $(12.8, 0.11)$ for suburban, urban, and dense urban environments, respectively. As we can see, in both cellular and cell-free schemes, the suburban environment outperforms the urban and dense urban environments, and the dense urban environment performs the worst. This is due to the higher probability of establishing a LoS link in suburban environment. Also, one can see that the proposed cell-free scheme performs better than the baseline cellular scheme for all

¹Note that for simulations, we utilize these heuristic solutions as the initial points in Algorithm 2 and Algorithm 3 for powers and locations of the UxNBs.

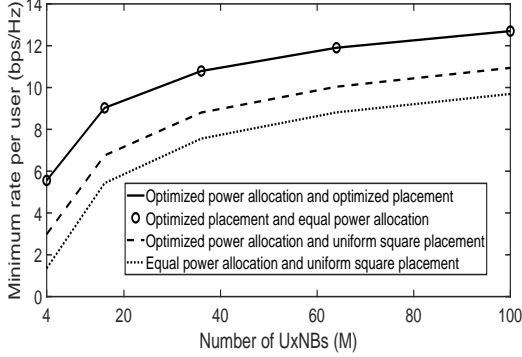


Fig. 9: The achievable minimum rate per user in the proposed cell-free scheme versus number of UxNBs (M) for the cases where the locations of UxNBs and/or allocated power for each user at each UxNB are optimized. We assumed that $K = 16$, $P_m = 25$ dBm, $\forall m$, $S = 400$, $N = 4$, and $G = 9$.

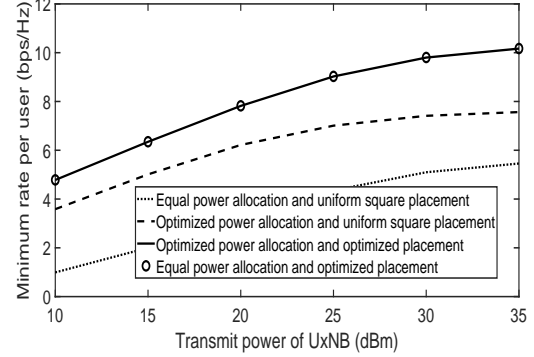


Fig. 10: The achievable minimum rate per user in the proposed cell-free scheme versus total power of each UxNB ($P_1 = \dots = P_M$), for the cases where the locations of UxNBs and/or allocated power for each user at each UxNB are optimized. We assumed that $K = 16$, $M = 16$, $S = 400$, $N = 4$, and $G = 9$.

environments, and this is due to the utilization of all the received signals from all users at each UxNB in the cell-free mode.

Fig. 12 shows the achievable minimum rate per user versus the number of UxNBs (M) in aerial schemes for three urban, suburban, and dense urban environments. As we can see, the proposed aerial cell-free scheme outperforms the aerial cellular scheme for all environments. We can also see that by increasing M , the performance of both cell-free and cellular schemes improves for all environments, and this is due to the establishment of more LoS links between the UxNBs and users for a larger M in aerial schemes. Further, it is shown that the superiority of the proposed cell-free scheme over the aerial cellular scheme for all environments increases by M , and this is due to a higher intercell interference for the cellular scheme at a higher value for M .

Simulation results showed that the aerial cell-free scheme performs much better than the terrestrial cell-free scheme when the HAPS is equipped with a very large antenna array. This performance increase comes at the cost of deploying a HAPS and dedicated UAVs. In order to reduce the UAV deployment costs, we can utilize other non-dedicated UAVs as UxNBs by equipping them with the proposed transceiver scheme. In regard to deploying a HAPS, it should be noted that HAPS can be deployed in the stratosphere for many other use cases, such as super

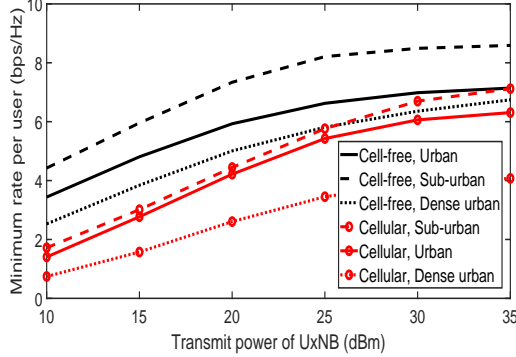


Fig. 11: The achievable minimum rate per user versus total power of each UxNB ($P_1 = \dots = P_M$) in aerial schemes for three urban, suburban, and dense urban environments. We set $K = 16$, $M = 16$, $N = 4$, $S = 400$, and $G = 9$.

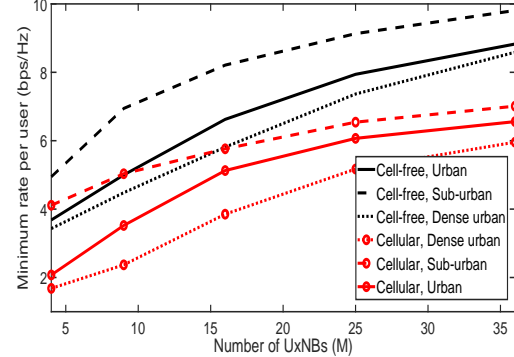


Fig. 12: The achievable minimum rate per user versus the number of UxNBs (M) in aerial schemes for three urban, suburban, and dense urban environments. We set $P_m = 25$ dBm, $\forall m$, $K = 16$, $N = 4$, $S = 400$, and $G = 9$.

macro BS, RSS, computing, sensing, and localization, and in this paper it is utilizes as a CPU as well. Finally, it should be noted that despite the costs of deploying UAVs and a HAPS, there are some application scenarios where the proposed scheme may nevertheless be advantageous, such as providing a dedicated service for wealthy users, offloading from saturated terrestrial networks, and special events involving a massive number of users.

VI. CONCLUSION

In this paper, we proposed a cell-free scheme for a set of UxNBs to manage the severe interference in aerial cellular networks between terrestrial users and UxNBs of neighboring cells. We also proposed to use a HAPS as a CPU to combine all the received signals from all UxNBs in the sub-THz band. This involved proposing a transceiver scheme at the UxNBs, a receiver scheme at the HAPS, and formulating an optimization problem to maximize the minimum SINR of users. Simulation results proved the superiority of the proposed scheme compared to aerial cellular and terrestrial cell-free baseline schemes in urban, suburban, and dense urban environments, which is due to the existence of LoS links between users and UxNBs. Simulation results also showed that utilizing a HAPS as a CPU is useful when the considerable path loss in the sub-THz band between UxNBs and the HAPS is compensated for by a high number of antenna elements at the HAPS.

APPENDIX A

PROOF OF PROPOSITION 1

In order to derive the SINR of each user, we rewrite the filtered and combined signal at RB k in the HAPS, i.e., y^k in (8), as

$$\begin{aligned}
y^k &= \sum_{m=1}^M \sum_{s=1}^S c_{ms}^* y_s^k = \sum_{m=1}^M \sum_{s=1}^S c_{ms}^* \left(P \sum_{m'=1}^M c_{m's} \gamma_{m'} y_{km'} + z_H \right) = \sum_{m=1}^M \sum_{s=1}^S c_{ms}^* \left(P \sum_{m'=1}^M c_{m's} \gamma_{m'} \sqrt{P_{km'}} y_{km'}^{\text{NORM}} + z_H \right) \\
&= \sum_{m=1}^M \sum_{s=1}^S c_{ms}^* \left(P \sum_{m'=1}^M c_{m's} \gamma_{m'} \sqrt{P_{km'}} \frac{y_{km'}^{\text{COMB}}}{|y_{km'}^{\text{COMB}}|} + z_H \right) = \sum_{m=1}^M \sum_{s=1}^S c_{ms}^* \left(P \sum_{m'=1}^M c_{m's} \gamma_{m'} \sqrt{P_{km'}} \frac{\sum_{n=1}^N y_{km'n}^{\text{MF}}}{|\sum_{n=1}^N y_{km'n}^{\text{MF}}|} + z_H \right) \\
&= \sum_{m=1}^M \sum_{s=1}^S c_{ms}^* \left(P \sum_{m'=1}^M c_{m's} \gamma_{m'} \sqrt{P_{km'}} \frac{\sum_{n=1}^N y_{m'n} \times \frac{h_{km'n}^*}{|h_{km'n}|}}{|\sum_{n=1}^N y_{m'n} \times \frac{h_{km'n}^*}{|h_{km'n}|}|} + z_H \right) \\
&= \sum_{m=1}^M \sum_{s=1}^S c_{ms}^* \left(P \sum_{m'=1}^M c_{m's} \gamma_{m'} \sqrt{P_{km'}} \frac{\sum_{n=1}^N (\sum_{k'=1}^K h_{k'm'n} \sqrt{P_{k'}} s_{k'} + z_{m'}) \times \frac{h_{km'n}^*}{|h_{km'n}|}}{|\sum_{n=1}^N (\sum_{k'=1}^K h_{k'm'n} \sqrt{P_{k'}} s_{k'} + z_{m'}) \times \frac{h_{km'n}^*}{|h_{km'n}|}|} + z_H \right). \tag{37}
\end{aligned}$$

Then, with the use-and-then-forget bound [38], we derive the achievable SINR. From the last equation of (37), we write the desired signal (DS) for user k as

$$\begin{aligned}
\text{DS}_k &= \sum_{m=1}^M \sum_{s=1}^S c_{ms}^* P \sum_{m'=1}^M c_{m's} \gamma_{m'} \sqrt{P_{km'}} \frac{\sum_{n=1}^N h_{km'n} \sqrt{P_k} s_k \times \frac{h_{km'n}^*}{|h_{km'n}|}}{|\sum_{n=1}^N (\sum_{k'=1}^K h_{k'm'n} \sqrt{P_{k'}} s_{k'} + z_{m'}) \times \frac{h_{km'n}^*}{|h_{km'n}|}|} \\
&= \sum_{m=1}^M \sum_{s=1}^S c_{ms}^* P \sum_{m'=1}^M c_{m's} \gamma_{m'} \sqrt{P_{km'}} \frac{\sum_{n=1}^N |h_{km'n}| \sqrt{P_k} s_k}{|\sum_{n=1}^N (\sum_{k'=1}^K h_{k'm'n} \sqrt{P_{k'}} s_{k'} + z_{m'}) \times \frac{h_{km'n}^*}{|h_{km'n}|}|}. \tag{38}
\end{aligned}$$

The standard deviation of the power normalization factor, i.e., $|\sum_{n=1}^N (\sum_{k'=1}^K h_{k'm'n} \sqrt{P_{k'}} s_{k'} + z_{m'}) \times \frac{h_{km'n}^*}{|h_{km'n}|}|$, in the denominator of the desired signal in (38) is given by

$$\begin{aligned}
F_{\text{NORM}} &= \sqrt{E[(\frac{1}{M} \sum_{m=1}^M \sum_{n=1}^N (\sum_{k'=1}^K h_{k'm'n} \sqrt{P_{k'}} s_{k'} + z_{m'}) \times \frac{h_{kmn}^*}{|h_{kmn}|})(\frac{1}{M} \sum_{m=1}^M \sum_{n=1}^N (\sum_{k'=1}^K h_{k'm'n} \sqrt{P_{k'}} s_{k'} + z_{m'}) \times \frac{h_{kmn}^*}{|h_{kmn}|})^*]} \\
&= \frac{1}{M} \sqrt{E[\sum_{m=1}^M \sum_{n=1}^N (\sum_{k'=1}^K |h_{k'm'n}|^2 P_{k'} |s_{k'}|^2 + |z_m|^2)]} = \frac{1}{M} \sqrt{\sum_{m=1}^M \sum_{n=1}^N (\sum_{k'=1}^K E[|h_{k'm'n}|^2] P_{k'} E[|s_{k'}|^2] + E[|z_m|^2])} \\
&= \frac{1}{M} \sqrt{\sum_{m=1}^M \sum_{n=1}^N (\sum_{k'=1}^K \beta_{k'm}^2 P_{k'} + \sigma^2)} = \frac{\sqrt{N}}{M} \sqrt{\sum_{m=1}^M \sum_{k'=1}^K \beta_{k'm}^2 P_{k'} + M\sigma^2}. \tag{39}
\end{aligned}$$

The expectation of the desired signal for user k can then be written as

$$\begin{aligned}
E[\text{DS}_k] &= E[\frac{1}{F_{\text{NORM}}} \sum_{m=1}^M \sum_{s=1}^S c_{ms}^* G \sum_{m'=1}^M c_{m's} \gamma_{m'} \sqrt{P_{km'}} \sum_{n=1}^N |h_{km'n}| \sqrt{P_k}] = \frac{G \sqrt{P_k}}{F_{\text{NORM}}} \sum_{m=1}^M \sum_{s=1}^S |c_{ms}|^2 \gamma_m \sqrt{P_{km}} \sum_{n=1}^N E[|h_{kmn}|] \\
&= \frac{G \sqrt{P_k}}{F_{\text{NORM}}} \sum_{m=1}^M \sum_{s=1}^S \gamma_m \sqrt{P_{km}} \sum_{n=1}^N \beta_{km} = \frac{G N S \sqrt{P_k}}{F_{\text{NORM}}} \sum_{m=1}^M \gamma_m \sqrt{P_{km}} \beta_{km}. \tag{40}
\end{aligned}$$

Next, we derive the variance of the interference terms in (37). We can see there that we have two types of interference. The first type is caused by interference from other users, and we show

it with $I_{k,U}$. The second type is due to the amplified noise at UxNBs, and we name it $I_{k,N}$. For $I_{k,U}$, we can write

$$\begin{aligned}
E[I_{k,U} \times I_{k,U}^*] &= E\left[\left(\frac{1}{F_{\text{NORM}}} \sum_{m=1}^M \sum_{s=1}^S c_{ms}^* G \sum_{m'=1}^M c_{m's} \gamma_{m'} \sqrt{P_{km'}} \sum_{n=1}^N \sum_{k'=1}^K h_{k'm'n} \sqrt{P_{k'}} s_{k'} \times \frac{h_{k'm'n}^*}{|h_{k'm'n}|}\right)\right. \\
&\quad \times \left.\left(\frac{1}{F_{\text{NORM}}} \sum_{m=1}^M \sum_{s=1}^S c_{ms}^* G \sum_{m'=1}^M c_{m's} \gamma_{m'} \sqrt{P_{km'}} \sum_{n=1}^N \sum_{k'=1}^K h_{k'm'n} \sqrt{P_{k'}} s_{k'} \times \frac{h_{k'm'n}^*}{|h_{k'm'n}|}\right)^*\right] \\
&= \frac{G^2}{F_{\text{NORM}}^2} \sum_{m=1}^M \sum_{s=1}^S c_{ms}^* c_{ms} c_{ms} c_{ms}^* \gamma_m^2 P_{km} \sum_{n=1}^N \sum_{k'=1}^K E[h_{k'mn} h_{k'mn}^*] P_{k'} E[|s_{k'}|^2] \times \frac{h_{k'mn}^*}{|h_{k'mn}|} \frac{h_{k'mn}}{|h_{k'mn}|} \\
&= \frac{SG^2}{F_{\text{NORM}}^2} \sum_{m=1}^M \gamma_m^2 P_{km} \sum_{n=1}^N \sum_{k'=1}^K \beta_{k'm}^2 P_{k'} = \frac{NSG^2}{F_{\text{NORM}}^2} \sum_{m=1}^M \gamma_m^2 P_{km} \sum_{k'=1}^K \beta_{k'm}^2 P_{k'}.
\end{aligned} \tag{41}$$

Also, for the variance of the $I_{k,N}$, we can write

$$\begin{aligned}
E[I_{k,N} I_{k,N}^*] &= \frac{1}{F_{\text{NORM}}^2} E\left[\left(\sum_{m=1}^M \sum_{s=1}^S c_{ms}^* G \sum_{m'=1}^M c_{m's} \gamma_{m'} \sqrt{P_{km'}} \sum_{n=1}^N z_{m'} \times \frac{h_{k'm'n}^*}{|h_{k'm'n}|}\right)\right. \\
&\quad \times \left.\left(\sum_{m=1}^M \sum_{s=1}^S c_{ms}^* G \sum_{m'=1}^M c_{m's} \gamma_{m'} \sqrt{P_{km'}} \sum_{n=1}^N z_{m'} \times \frac{h_{k'm'n}^*}{|h_{k'm'n}|}\right)^*\right] \\
&= \frac{G^2}{F_{\text{NORM}}^2} \sum_{m=1}^M \sum_{s=1}^S c_{ms}^* c_{ms} c_{ms} c_{ms}^* \gamma_m^2 P_{km} \sum_{n=1}^N E[|z_m|^2] \times \frac{h_{k'mn}^*}{|h_{k'mn}|} \frac{h_{k'mn}}{|h_{k'mn}|} = \frac{NSG^2}{F_{\text{NORM}}^2} \sum_{m=1}^M \gamma_m^2 P_{km} \sigma^2.
\end{aligned} \tag{42}$$

Finally, we show the noise at the HAPS with N_{HAPS} , whose variance is given by

$$E[N_{\text{HAPS}} N_{\text{HAPS}}^*] = E\left[\sum_{m=1}^M \sum_{s=1}^S c_{ms}^* z_H \times \left(\sum_{m=1}^M \sum_{s=1}^S c_{ms}^* z_H\right)^*\right] = \sum_{m=1}^M \sum_{s=1}^S c_{ms}^* c_{ms} E[|z_H|^2] = MS\sigma_H^2. \tag{43}$$

As we mention in Section II, in the sub-THz band, the absorbed parts of the signals by the medium are re-emitted with a random phase shift [23], [33]. Due to its random phase, this re-emission interference signal, that is indicated by $I_{k,R}$ for user k , is uncorrelated with y^k in (37), and its mean value is equal to 0. In order to get the variance of the re-emission interference for user k , we just need to replace the terms $\gamma_m^2 = \tau_m \rho_m^2$ with $(1 - \tau_m) \rho_m^2$ in the variance expressions of the interference formulas in (37), i.e., $E[I_{k,U} \times I_{k,U}^*]$ in (41) and $E[I_{k,N} \times I_{k,N}^*]$ in (42), and combine them as follows:

$$E[I_{k,R} I_{k,R}^*] = \frac{NSG^2}{F_{\text{NORM}}^2} \sum_{m=1}^M (1 - \tau_m) \rho_m^2 P_{km} \sum_{k'=1}^K \beta_{k'm}^2 P_{k'} + \frac{NSG^2}{F_{\text{NORM}}^2} \sum_{m=1}^M (1 - \tau_m) \rho_m^2 P_{km} \sigma^2. \tag{44}$$

Now, according to the derived formulas for $E[\text{DS}_k]$, $E[I_{k,U} \times I_{k,U}^*]$, $E[I_{k,N} \times I_{k,N}^*]$, $E[N_{\text{HAPS}} N_{\text{HAPS}}^*]$, and $E[I_{k,R} I_{k,R}^*]$, we derive the SINR of the user k for the proposed scheme as follows:

$$\begin{aligned}
\text{SINR}_k &= \frac{E[\text{DS}_k]^2}{E[I_{k,U} I_{k,U}^*] + E[I_{k,N} I_{k,N}^*] + E[I_{k,R} I_{k,R}^*] + E[N_{\text{HAPS}} N_{\text{HAPS}}^*]} \\
&= \frac{\left(\frac{GNS\sqrt{P_k}}{F_{\text{NORM}}} \sum_{m=1}^M \gamma_m \sqrt{P_{km}} \beta_{km}\right)^2}{\frac{NSG^2}{F_{\text{NORM}}^2} \sum_{m=1}^M \rho_m^2 P_{km} \sum_{k'=1}^K \beta_{k'm}^2 P_{k'} + \frac{NSG^2}{F_{\text{NORM}}^2} \sum_{m=1}^M \rho_m^2 P_{km} \sigma^2 + MS\sigma_H^2} \\
&= \frac{G^2 N^2 S P_k \left(\sum_{m=1}^M \gamma_m \sqrt{P_{km}} \beta_{km}\right)^2}{NG^2 \sum_{m=1}^M \rho_m^2 P_{km} \sum_{k'=1}^K \beta_{k'm}^2 P_{k'} + NG^2 \sum_{m=1}^M \rho_m^2 P_{km} \sigma^2 + M\sigma_H^2 F_{\text{NORM}}^2} \\
&= \frac{G^2 N^2 S P_k \left(\sum_{m=1}^M \gamma_m \sqrt{P_{km}} \beta_{km}\right)^2}{NG^2 \sum_{m=1}^M \rho_m^2 P_{km} \sum_{k'=1}^K \beta_{k'm}^2 P_{k'} + NG^2 \sum_{m=1}^M \rho_m^2 P_{km} \sigma^2 + M\sigma_H^2 \left(\frac{\sqrt{N}}{M} \sqrt{\sum_{m=1}^M \sum_{k'=1}^K \beta_{k'm}^2 P_{k'}} + M\sigma^2\right)^2} \\
&= \frac{MG^2 N S P_k \left(\sum_{m=1}^M \gamma_m \sqrt{P_{km}} \beta_{km}\right)^2}{MG^2 \sum_{m=1}^M \rho_m^2 P_{km} \sum_{k'=1}^K \beta_{k'm}^2 P_{k'} + MG^2 \sum_{m=1}^M \rho_m^2 P_{km} \sigma^2 + \sigma_H^2 \left(\sum_{m=1}^M \sum_{k'=1}^K \beta_{k'm}^2 P_{k'} + M\sigma^2\right)^2}.
\end{aligned} \tag{45}$$

Utilizing these SINRs, we can derive the achievable rate of user k as $R_k = \log_2(1 + \text{SINR}_k)$, and the proof is completed.

APPENDIX B PROOF OF PROPOSITION 2

In order to prove the quasi-concavity of (P1), we need to show that the objective function is quasi-concave, and that the constraints' set is convex. To prove quasi-concavity of the objective function, we just need to prove that its upper-level set is a convex set [26]. For this, we first perform the variable change $\mathbf{T} = [P_{km}^2]_{K \times M}$ in (P1) and show the objective function with $f(\mathbf{T})$. Hence, for any $t \in \mathbb{R}_+$, the upper-level set (ULS) of the objective function will be

$$\begin{aligned}
 \text{ULS}(f, t) &= \{T : f(T) > t\} \\
 &= \left\{ T : \frac{MP^2NSP_k(\sum_{m=1}^M \gamma_m T_{km} \beta_{km})^2}{MP^2 \sum_{m=1}^M \rho_m^2 T_{km}^2 \sum_{k'=1}^K \beta_{k'm}^2 P_{k'} + MP^2 \sum_{m=1}^M \rho_m^2 T_{km}^2 \sigma^2 + \sigma_H^2 (\sum_{m=1}^M \sum_{k'=1}^K \beta_{k'm}^2 P_{k'} + M\sigma^2)} > t, \forall k \right\} \\
 &= \left\{ T : \sqrt{MP^2 \sum_{m=1}^M \rho_m^2 T_{km}^2 \sum_{k'=1}^K \beta_{k'm}^2 P_{k'} + MP^2 \sum_{m=1}^M \rho_m^2 T_{km}^2 \sigma^2 + \sigma_H^2 (\sum_{m=1}^M \sum_{k'=1}^K \beta_{k'm}^2 P_{k'} + M\sigma^2)} \right. \\
 &\quad \left. < \frac{\sqrt{MP^2NSP_k} \sum_{m=1}^M \gamma_m T_{km} \beta_{km}}{\sqrt{t}}, \forall k \right\}.
 \end{aligned} \tag{46}$$

We can see that this set is in the form of a norm function less than an affine function of variable T , and hence it is a convex set. With the new variable T , the constraint (20) will be $\sum_{k=1}^K T_{km}^2 \leq P_m, \forall m$, which is a convex set, and the proof is completed.

REFERENCES

- [1] 3GPP TR 22.829, “Enhancement for unmanned aerial vehicles (UAVs),” *3rd Generation Partnership Project*, 2019.
- [2] L. Liu, S. Zhang, and R. Zhang, “CoMP in the sky: UAV placement and movement optimization for multi-user communications,” *IEEE Transactions on Communications*, vol. 67, no. 8, pp. 5645–5658, Aug. 2019.
- [3] E. Kalantari, M. Z. Shakir, H. Yanikomeroglu, and A. Yongacoglu, “Backhaul-aware robust 3D drone placement in 5G+ wireless networks,” in *2017 IEEE International Conference on Communications Workshops (ICC Workshops)*, pp. 109–114.
- [4] E. Nayebi, A. Ashikhmin, T. L. Marzetta, H. Yang, and B. D. Rao, “Precoding and power optimization in cell-free massive MIMO systems,” *IEEE Transactions on Wireless Communications*, vol. 16, no. 7, pp. 4445–4459, Jul. 2017.
- [5] G. Karabulut Kurt, M. G. Khoshkhogh, S. Alfattani, A. Ibrahim, T. S. J. Darwish, M. S. Alam, H. Yanikomeroglu, and A. Yongacoglu, “A vision and framework for the high altitude platform station (HAPS) networks of the future,” *IEEE Communications Surveys and Tutorials*, vol. 23, no. 2, pp. 729–779, Secondquarter 2021.
- [6] H. Q. Ngo, A. Ashikhmin, H. Yang, E. G. Larsson, and T. L. Marzetta, “Cell-free massive MIMO versus small cells,” *IEEE Transactions on Wireless Communications*, vol. 16, no. 3, pp. 1834–1850, Mar. 2017.

- [7] M. Bashar, K. Cumanan, A. G. Burr, M. Debbah, and H. Q. Ngo, "On the uplink max–min SINR of cell-free massive MIMO systems," *IEEE Transactions on Wireless Communications*, vol. 18, no. 4, pp. 2021–2036, Apr. 2019.
- [8] M. Bashar, K. Cumanan, A. G. Burr, H. Q. Ngo, and M. Debbah, "Cell-free massive MIMO with limited backhaul," in *2018 IEEE International Conference on Communications (ICC)*, pp. 1–7.
- [9] E. Kalantari, H. Yanikomeroglu, and A. Yongacoglu, "Wireless networks with cache-enabled and backhaul-limited aerial base stations," *IEEE Transactions on Wireless Communications*, vol. 19, no. 11, pp. 7363–7376, Nov. 2020.
- [10] B. Galkin, J. Kibilda, and L. A. DaSilva, "Backhaul for low-altitude UAVs in urban environments," in *2018 IEEE International Conference on Communications (ICC)*, pp. 1–6.
- [11] M. Gapeyenko, V. Petrov, D. Moltchanov, S. Andreev, N. Himayat, and Y. Koucheryavy, "Flexible and reliable UAV-assisted backhaul operation in 5G mmwave cellular networks," *IEEE Journal on Selected Areas in Communications*, vol. 36, no. 11, pp. 2486–2496, Nov. 2018.
- [12] 3GPP TR 38.811, "Study on new radio (NR) to support non-terrestrial networks," *3rd Generation Partnership Project*, 2020.
- [13] Y. Shibata, N. Kanazawa, M. Konishi, K. Hoshino, Y. Ohta, and A. Nagate, "System design of gigabit HAPS mobile communications," *IEEE Access*, vol. 8, pp. 157 995–158 007, Aug. 2020.
- [14] D. Grace and M. Mohorcic, *Broadband Communications via High Altitude Platforms*. John Wiley & Sons, 2011.
- [15] M. S. Alam, G. K. Kurt, H. Yanikomeroglu, P. Zhu, and N. D. Dao, "High altitude platform station based super macro base station constellations," *IEEE Communications Magazine*, vol. 59, no. 1, pp. 103–109, Jan. 2021.
- [16] Q. Ren, O. Abbasi, G. K. Kurt, H. Yanikomeroglu, and J. Chen, "Caching and computation offloading in high altitude platform station (HAPS) assisted intelligent transportation systems," *arXiv preprint arXiv:2106.14928*, 2021.
- [17] G. Karabulut Kurt and H. Yanikomeroglu, "Communication, computing, caching, and sensing for next-generation aerial delivery networks: Using a high-altitude platform station as an enabling technology," *IEEE Vehicular Technology Magazine*, vol. 16, no. 3, pp. 108–117, Sep. 2021.
- [18] S. Alfattani, W. Jaafar, Y. Hmamouche, H. Yanikomeroglu, and A. Yongaçoglu, "Link budget analysis for reconfigurable smart surfaces in aerial platforms," *IEEE Open Journal of the Communications Society*, vol. 2, pp. 1980–1995, Aug. 2021.
- [19] A.-A. A. Boulogeorgos, A. Alexiou, T. Merkle, C. Schubert, R. Elschner, A. Katsiotis, P. Stavrianos, D. Kritharidis, P.-K. Chartsias, J. Kokkoniemi, M. Juntti, J. Lehtomaki, A. Teixeira, and F. Rodrigues, "Terahertz technologies to deliver optical network quality of experience in wireless systems beyond 5G," *IEEE Communications Magazine*, vol. 56, no. 6, pp. 144–151, Jun. 2018.
- [20] I. F. Akyildiz, J. M. Jornet, and C. Han, "Terahertz band: Next frontier for wireless communications," *Physical communication*, vol. 12, pp. 16–32, Sep. 2014.
- [21] J. Kokkoniemi, J. Lehtomäki, and M. Juntti, "A line-of-sight channel model for the 100–450 gigahertz frequency band," *EURASIP Journal on Wireless Communications and Networking*, vol. 2021, no. 1, pp. 1–15, Apr. 2021.
- [22] T. S. Rappaport, Y. Xing, O. Kanhere, S. Ju, A. Madanayake, S. Mandal, A. Alkhateeb, and G. C. Trichopoulos, "Wireless communications and applications above 100 GHz: Opportunities and challenges for 6G and beyond," *IEEE Access*, vol. 7, pp. 78 729–78 757, Jun. 2019.
- [23] V. Petrov, D. Moltchanov, and Y. Koucheryavy, "Interference and SINR in dense terahertz networks," in *2015 IEEE 82nd Vehicular Technology Conference (VTC-Fall)*, pp. 1–5.
- [24] A. Liao, Z. Gao, D. Wang, H. Wang, H. Yin, D. W. K. Ng, and M.-S. Alouini, "Terahertz ultra-massive MIMO-based aeronautical communications in space-air-ground integrated networks," *IEEE Journal on Selected Areas in Communications*, vol. 39, no. 6, pp. 1741–1767, Jun. 2021.

- [25] L. Xu, M. Chen, M. Chen, Z. Yang, C. Chaccour, W. Saad, and C. S. Hong, “Joint location, bandwidth and power optimization for THz-enabled UAV communications,” *IEEE Communications Letters*, vol. 25, no. 6, pp. 1984–1988, Jun. 2021.
- [26] A. Agrawal and S. Boyd, “Disciplined quasiconvex programming,” *Optimization Letters*, vol. 14, no. 7, pp. 1643–1657, 2020.
- [27] S. Boyd, S. P. Boyd, and L. Vandenberghe, *Convex Optimization*. Cambridge University Press, 2004.
- [28] M. Razaviyayn, M. Hong, and Z.-Q. Luo, “A unified convergence analysis of block successive minimization methods for nonsmooth optimization,” *SIAM Journal on Optimization*, vol. 23, no. 2, pp. 1126–1153, 2013.
- [29] Z. Chen and E. Björnson, “Channel hardening and favorable propagation in cell-free massive MIMO with stochastic geometry,” *IEEE Transactions on Communications*, vol. 66, no. 11, pp. 5205–5219, Nov. 2018.
- [30] A. Al-Hourani, S. Kandeepan, and S. Lardner, “Optimal LAP altitude for maximum coverage,” *IEEE Wireless Communications Letters*, vol. 3, no. 6, pp. 569–572, Dec. 2014.
- [31] R. I. Bor-Yaliniz, A. El-Keyi, and H. Yanikomeroglu, “Efficient 3-D placement of an aerial base station in next generation cellular networks,” in *2016 IEEE International Conference on Communications (ICC)*, pp. 1–5.
- [32] P. Series, “Attenuation by atmospheric gases and related effects,” *Recommendation ITU-R*, pp. 676–12, 2019.
- [33] C. Chaccour, R. Amer, B. Zhou, and W. Saad, “On the reliability of wireless virtual reality at terahertz (THz) frequencies,” in *2019 10th IFIP International Conference on New Technologies, Mobility and Security (NTMS)*, pp. 1–5.
- [34] O. Abbasi, A. Ebrahimi, and N. Mokari, “NOMA inspired cooperative relaying system using an AF relay,” *IEEE Wireless Communications Letters*, vol. 8, no. 1, pp. 261–264, Feb. 2019.
- [35] S. Ahmadi, *5G NR: Architecture, Technology, Implementation, and Operation of 3GPP New Radio Standards*. Academic Press, 2019.
- [36] 3GPP TR 38.801, “Study on new radio access technology: radio access architecture and interfaces,” *3rd Generation Partnership Project*, 2017.
- [37] O. Abbasi, H. Yanikomeroglu, A. Ebrahimi, and N. M. Yamchi, “Trajectory design and power allocation for drone-assisted NR-V2X network with dynamic NOMA/OMA,” *IEEE Transactions on Wireless Communications*, vol. 19, no. 11, pp. 7153–7168, Nov. 2020.
- [38] T. L. Marzetta, *Fundamentals of Massive MIMO*. Cambridge University Press, 2016.